Electronic Supplementary Information (ESI):

Non-covalent Interaction of Benzene with Methanol and Diethyl Ether Solid Surfaces†

Demian Marchione*[a] and Martin R. S. McCoustra[a]

1 TPD Experiments

Raw temperature programmed desorption (TPD) data appear to be the combination of two signals; one is desorption from the sample mount, more precisely from the heating wires, while the other corresponds to sublimation of the sample from the substrate. Any distinction between these two becomes less marked at large exposures because the signal derived from the wires does not decay quickly enough to zero and overlaps with the incipient desorption from the sample. In order to resolve the two signals from one another, the experimental points at base temperature and those in the leading edge region were fitted with an exponential function (**Figure S1**). The resulting curve was then used to estimate

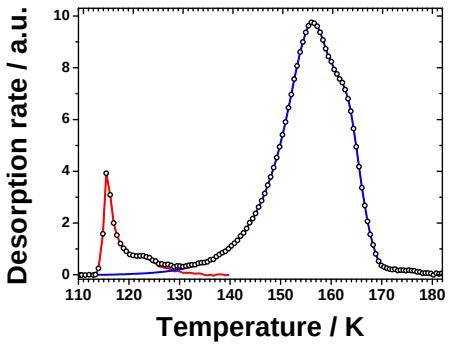

Figure S1: *TPD traces of 0.5 L of C_6H_6 deposited on a thick CH_3OH film (200 L). The contribution to the overall signal from the wires and the substrate are reported with red and blue lines respectively, while the raw data as black open circles.*

the signal from the wires and subtracted from the overall trace to give a "cleaned" trace, which should be a reasonable representation of the TPD trace specific to the substrate. This procedure has the drawback of forcing a mono-exponential trend that describes the desorption rate over a certain temperature range where the leading edge of the desorption

*[a] *Institute of Chemical Sciences, Heriot-Watt University, EH14 4AS, Edinburgh, UK; E-mail: marchionedemian@gmail.com*
[a] *Institute of Chemical Sciences, Heriot-Watt University, EH14 4AS, Edinburgh, UK; E-mail: mrsm1@hw.ac.uk*

peak is most sensitive. The more benzene (C_6H_6) is deposited, the larger is the error introduced by the fitting function simply because the overlap between the two features becomes more and more significant.

This procedure affects the leading edge analysis especially when applied to TPD curves corresponding to higher C_6H_6 exposures. Therefore, we can only attempt a semi-quantitative analysis for peak A in **Figure 1** of the article as displayed by the Arrhenius plots in **Figure S2** corresponding to the TPD traces between 0.02 L and 0.5 L of C_6H_6 on 200 L of CH_3OH. The Arrhenius plots were obtained by rewriting the Polanyi-Wigner equation,

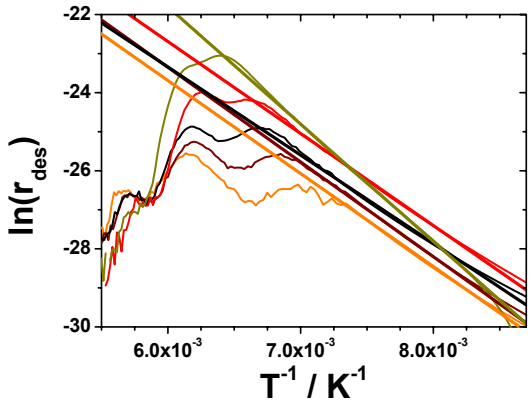

Figure S2: *Arrhenius plots of $ln(r_{des})$ against 1/T corresponding to the TPD traces of C_6H_6 on 200 L of CH_3OH. C_6H_6 exposures are 0.02 L (orange), 0.05 L (brown), 0.1 L (black), 0.2 L (red), 0.5 L (dark yellow) The best linear fit is reported along the experimental traces, and for each coverage going from the lowest dose to the highest, the desorption energies are: 20 ± 2 kJ mol^{-1}, 20 ± 2 kJ mol^{-1}, 19 ± 2 kJ mol^{-1}, 20 ± 2 kJ mol^{-1}, 25 ± 2 kJ mol^{-1}.*

eqn (1a),[1,2] in its logarithmic form as a function of 1/T, eqn (1b):

$$r_{des} = -\frac{dN_{ads}}{dt} = \frac{\nu_n N_{ads}^n}{\beta} e^{-\frac{E_{des}}{RT}} \tag{1a}$$

$$ln(r_{des}) = ln\left(\frac{\nu_n}{\beta}\right) + ln\left(N_{ads}^n\right) - \left(\frac{E_{des}}{R}\right) \times \frac{1}{T} \tag{1b}$$

where r_{des} is desorption rate, N_{ads} is the surface coverage of adsorbate in molecules cm^{-2}, ν_n is the pre-exponential factor for a desorption process having order n, β is the heating rate in K s^{-1}, E_{des} is the desorption energy in J mol^{-1}, R is the gas constant in J K^{-1} mol^{-1}, and T is the temperature. Analysis using eqn (1b) yields a straight line in the leading edge region with the slope containing the desorption energy, E_{des}. It follows that a value of 21 ± 2 kJ mol^{-1} is obtained for the desorption energy of Peak A. It should be stressed once again that in order to deconvolve the the signal coming from the sample

mounting and desorption from the substrate itself, the data had to be carefully processed. This procedure may have particularly affected the 0.5 L trace (highest coverage used for the analysis) resulting in a desorption energy (25 ± 2 kJ mol^{-1}) that is slightly larger than the average value (21 ± 2 kJ mol^{-1}). However, whether this value is discarded or not, the average remains unchanged within the error bars.

Furthermore, we tried to fit the TPD traces displayed in **Figure 1** of the main article using Gaussian or Lorentzian functions. However, the results showed no improvement to the analysis of the data, but the procedure actually added more sources of error. For instance, one attempt was to fit each peak (A, B and C) with a Gaussian, while keeping C constant. However, as the benzene dose increases, the fitting procedure tends to "compress" the Gaussian corresponding to peak A (**Figure S3**) resulting in an unnatural behaviour that has no real physical meaning and has the only advantage of reducing the χ^2.

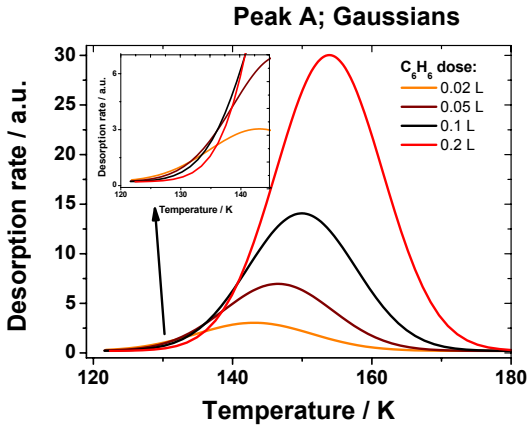

Figure S3: *Gaussian fits for peak A observed in the TPD traces of C_6H_6 on 200 L of CH_3OH. C_6H_6 exposures are 0.02 L (orange), 0.05 L (brown), 0.1 L (black), and 0.2 L (red). The inset highlights the unnatural narrowing of the Gaussian in order to improve the fit of the cumulative peak with the experimental trace.*

Furthermore, given the fact that this feature has a nearly zero-order desorption kinetics, then a Gaussian or a Lorentzian would not accurately describe the whole desorption profile. Most importantly, the systematic change in the leading edge of the fitting function as a function of the C_6H_6 dose would severely affect a leading edge analysis; perhaps even more than the method originally employed in the manuscript. Even using Lorentzian functions brought no improvement to the description of Peak A in any way (results not shown). In conclusion, it is not feasible to isolate the contributions to the desorption profile (peak A and B) by using standard fitting functions (*e.g.* Gaussian and Lorentzians). Perhaps kinetic simulations would be needed in order to correctly isolate and model the experimental data.

Peak B in **Figure 1** of the main article is assigned to strongly hydrogen bonded C_6H_6

molecules at the CH_3OH interface. The corresponding desorption energy was estimated by using the Redhead equation.[3] Depending on what value is chosen for the pre-exponential factor (ν_1), 10^{12} s^{-1} or 10^{13} s^{-1}, two possible estimates of E_{des} are possible: 39 $\pm$1 kJ mol^{-1} and 42 $\pm$ 1 kJ mol^{-1}. In principle both the choices are sensible: 10^{12} s^{-1} is typically assumed for physisorbed species, whereas 10^{13} s^{-1} can be assumed for chemisorbed species. Hydrogen bonds represent a borderline situation, therefore both the values for ν_1 were employed in our analysis.

In the discussion of the TPD data corresponding to low exposures of C_6H_6 on a thick film of methanol (CH_3OH), we stressed that different desorption behaviours are observed when the same experiment is repeated multiple times. Inconsistency spans over the whole range of C_6H_6 exposures investigated (0.01 L - 50 L), with larger discrepancies at sub-monolayer level (0.01 L - 0.5 L). In the latter case, as also shown in **Figure 1** of the main article and in **Figure S4**, three features can be observed in the TPD traces up to 1 L: a low temperature peak between 140 K and 155 K, another peak between 160 K and 170 K, and a small high temperature shoulder above 170 K that is saturated already at 0.01 L. The first two peaks compete with each other as displayed in **Figure S4** for the 0.1 L

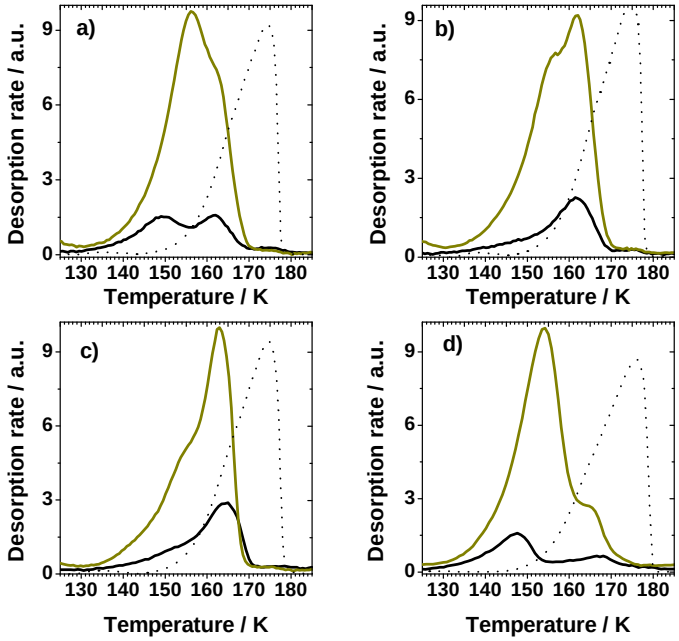

Figure S4: *TPD traces of 0.1 L (black line) and 0.5 L (dark yellow line) of C_6H_6 deposited on a thick CH_3OH film (200 L). The dotted line is the scaled CH_3OH TPD trace underlying the C_6H_6. The four replications show different outcomes of the experiment.*

and 0.5 L traces, resulting in four possible outcomes. In the upper panels the two features co-exist with the slight predominance of one over the other; in the lower panels only one of the two peaks clearly emerges while the other is just a shoulder. It should be noted that occasional variations of the heating ramp within the data set cannot explain the observed behaviour, which depends on small, unidentified changes in the experimental conditions (*e.g.* film deposition rate and structure). Therefore, an unusual number of replications of TPD experiments are required in order to obtain a consistent behaviour such as the one showed in **Figure 1** of the main article and allowing a more accurate determination of the desorption energies.

The TPD traces so far discussed and those displayed in the left panel of **Figure S5** correspond to C_6H_6 coverages in the sub-monolayer regime. In fact, assuming a layer-by-layer

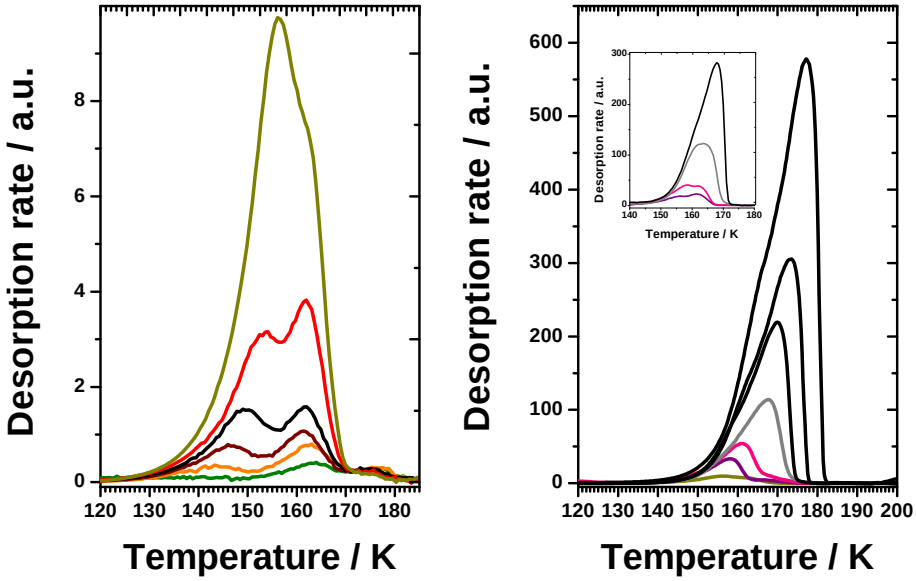

Figure S5: *TPD traces for C_6H_6 desorption from a thick ice of CH_3OH (200 L). The exposures of C_6H_6 that are displayed are: 0.01 L in green, 0.02 L in orange, 0.05 L in brown, 0.1 L in black, 0.2 L in red, 0.5 L in dark yellow. for the left panel. In the right panel C_6H_6 doses are 0.5 L, 1 L (in violet), 2 L (in pink) and 5 L (in dark grey), 10 L, 20 L and 50 L (in black). The inset shows an alternative desorption behaviour for the TPD traces corresponding to 1 L, 2 L, 5 L and 10 L of C_6H_6.*

growth mechanism, one monolayer corresponds to *ca.* 15 L. This is obtained by using the same procedure employed by Scott Smith *et al.* to define 1 monolayer of CH_3OH on graphene[4]. First we took the 2/3 root of the C_6H_6 molecular density[5] (8.57×10^{21} molecule cm^{-3}) and then compare this with $Z_W t$ as in **Equation 1** of the main article. However, such hypothesised growth mechanism was not observed for the investigated system, and hence, no precise exposure can be assigned to one uniform monolayer of C_6H_6

on CH_3OH. In contrast, it was possible to define the 5 L dose as an upper limit for the appearance of the multilayer because this is the highest exposure where the high temperature and the low temperature features might not be merged together (see inset in **Figure S5**). At 10 L and above only one peak, that corresponds to multilayer desorption, is noted (right panel of **Figure S5**).

Figure S6 displays the TPD data for 1 L, 2 L, 5 L and 10 L of diethyl ether (CH_3CH_2O-CH_2CH_3) on top of a thick C_6H_6 ice (200 L). The observed desorption behaviour is rather

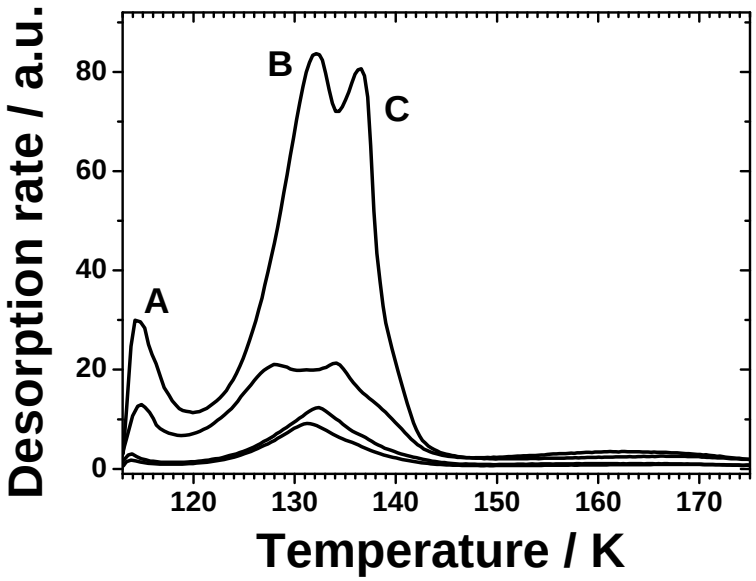

Figure S6: *TPD traces of 1 L, 2 L, 5 L and 10 L of $CH_3CH_2OCH_2CH_3$ deposited on a thick C_6H_6 film (200 L).*

complex and its detailed description is beyond the scope of the present work. However, there are few things that can be said. The sharp peak labelled as **A** is undesired signal from the sample mounting as already discussed. Peak **C** might correspond to desorption of a second layer of $CH_3CH_2OCH_2CH_3$. In **Figure 5** of the main article the temperature of the maximum shifts to lower values as the coverage increases up to 1 L. This trend is noted to change in **Figure S6**, when larger doses are taken into account, as the maximum of peak C moves towards higher temperatures going from 1 L up to 10 L. The lower temperature feature, Peak **B**, which appears at some point between 2 L and 5 L, grows rapidly in intensity by going from 5 L to 10 L and could be due to desorption of the multilayer. This assignment is proposed by comparison with TPD data (not shown) of $CH_3CH_2OCH_2CH_3$ pre-deposited directly on the steel substrate at similar coverages. The desorption behaviour of $CH_3CH_2OCH_2CH_3$ from steel is analogous to what observed on C_6H_6 with the sole difference of peak **C** which was not observed in the former case. In conclusion, it is clear

that regarding the $CH_3CH_2OCH_2CH_3/C_6H_6$ system, the transition towards the multilayer commences above 1 L, and hence the data presented in **Figure 4** of the main article are relevant to the sub-monolayer regime.

In addition to this, it is possible to estimate that 1 ML is equivalent to *ca.* 10 L, 9.2 L precisely. This was calculated in a similar fashion as it has been done with C_6H_6. First we assumed that the liquid bulk density (5.80×10^{21} molecules cm^{-3}) of $CH_3CH_2OCH_2CH_3$[1] was the same as in the pure solid. Then, by taking the 2/3 root of such molecular density as 1 ML we estimate that, for $CH_3CH_2OCH_2CH_3$, 1 ML is 9.2 L. Therefore, the exposures probed in **Figure 4** of the main article range between 0.005 ML and 0.1 ML. Given these very low fractional numbers and the assumption behind the definition of one equivalent monolayer, it is desirable to keep the notation based on raw exposure units (Langmuirs) which are plain and simple, free from any assumption of whichever sort. The case of the TPD data of ether on benzene are quite explanatory on this matter. As discussed for **Figure S6**, the desorption behaviour attributed to $CH_3CH_2OCH_2CH_3$ as multilayer appears at some point between 2 L and 5 L, whereas if one uses units of equivalent monolayer 9.2 L is identified as a complete monolayer. This equivalence can be misleading and is in contrast with what is shown by TPD data. In conclusion, in order to avoid misinterpretation of the data, Langmuir units are used throughout the main article instead of equivalent monolayers.

2 RAIR spectra

The multilayer RAIR spectrum of CH_3OH (200 L) deposited on the stainless steel substrate at base temperature is shown in **Figure S7**. The assignment of the vibrational modes is also reported in the figure caption and agrees well with literature values[6]. The frequency of the maximum for the CO stretch and its band-profile are consistent with the film being mainly amorphous. Following further annealing of the film at higher temperatures, e.g. 120 K for 100 s, the CO band splits and shifts towards lower wavenumbers consistently with the enhancement of the crystalline phase in the solid CH_3OH[7].

Figure S8 displays the multilayer RAIR spectrum corresponding to 200 L of CH_3CH_2O-CH_2CH_3 deposited on the steel substrate at *ca.* 107 K, consistently with a crystalline film. Maxima of the IR frequencies are listed in **Table S1** and match the reported data of $CH_3CH_2OCH_2CH_3$ on Ru(0001)[8] and on Cu(111)[9].

Figures S9 and **S10** display the evolution of the C_6H_6 IR signatures as the ice grows on

[1] Density of the liquid phase, Sigma-Aldrich

Assignment	IR Frequencies / cm^{-1}		
	This work	Ru(0001)[8]	Cu(111)[9]
$\rho(CH_3 + CH_2)$	822	827	830
	828		
$\nu_s(COC)$ [νCC]	843	849	848
	849		
	851		
$\nu(CC + CO) + \rho(CH_3)$	932	935	937
	940		
$2\rho(CH_3) + \nu(CC)$	1045	1048	1046
	1048		
$\nu_a(COC)$ [νCO]	1115	1120	1122
	1126		
$\rho(CH_3) + \nu(CO)$	1153	1159	1159
$+ \nu(CC)$ + bends	1159		
$\rho(CH_2 + CH_3)$	1170	1176	1178
	1175		
$\rho(CH_2)$ twist	1279	1283	1285
	1283		
$\delta_s(CH_3) + \delta(CH_2)_{o.p}$	1348	1346	1350
	1352		
$\delta_s(CH_3)$	1369	1370	1372
	1373		
$\delta_a(CH_3) + \delta(CH_2)_{o.p}$	1381	1382	1385
	1388		
$\delta_a(CH_3)_{o.p}$	1441	1441	1442
	1447		
$\delta_a(CH_3)_{i.p}$	1456		1459
	1459	1458	
	1468	1468	
$\delta_a(CH_2)$ scissoring	1498	1489	1491
$\nu_s(CH_3) + \nu_s(CH_2)$	2851, 2860	2856	
$+ 2 \times \delta(CH_3)$	2873	2872	2875
	2886, 2896	2900	
$\nu_a(CH_2)$	2932	2932	2934
$\nu_a(CH_3)$	2972 (2803)	2970	2971
	2982 (2777)	2987	2992
	2990 (2689, 2693)		

Table S1: *List of vibrational modes of 200 L of $CH_3CH_2OCH_2CH_3$ multilayer adsorbed on steel at 107 K. Out-of-plane modes are labelled with the initials o.p., while s. stands for symmetric and a. stands for asymmetric.*

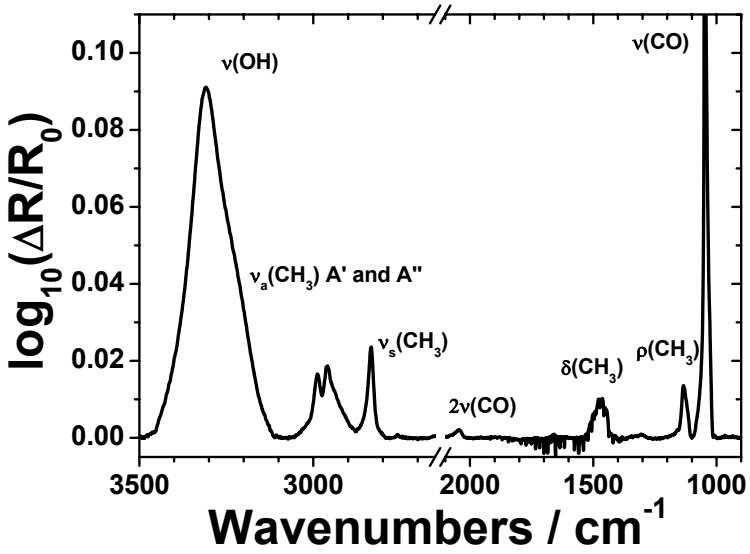

Figure S7: *RAIR spectrum of the multilayer CH_3OH film (200 L; $\sim$ 15.2 nm) grown on stainless steel at 107 K. CH_3OH vibrations are labelled as follows: $\nu(OH)$ is the OH stretching peaking at 3308 cm^{-1}; $\nu_a(CH_3)$ is the asymmetric methyl stretching mode with symmetry A' peaking at 2988 cm^{-1}; $\nu_a(CH_3)$ at 2959 cm^{-1} is the asymmetric methyl stretching mode with symmetry A''; $\nu_s(CH_3)$ at 2959 cm^{-1} is the symmetric methyl stretching mode centered at 2834 cm^{-1}; $2\nu(CO)$ is the CO stretching overtone at 2043 cm^{-1}; The methyl bend, δ (CH_3), is found at 1464 cm^{-1}, and might also include a minor contribution of the COH bending mode at $\sim$ 1510 cm^{-1}; $\rho(CH_3)$ is the rocking mode at 1134 cm^{-1}; $\nu(CO)$ is the CO stretching mode peaking at 1047 cm^{-1}. The negative sharp features between 1800 cm^{-1} and 1400 cm^{-1} are due to the bending modes of gaseous water (H_2O) in the air side of the chamber, in the IR path to the detector.*

top of a thick film of CH_3OH (200 L) or $CH_3CH_2OCH_2CH_3$ (200 L) respectively. These plots clearly show that only the ring modes are detected below 5 L of C_6H_6, while all the other bands appear in the multilayer regime between 5 L and 20 L. The assignment of the C_6H_6 modes is reported in **Table S2** and is based on the recorded spectra corresponding to the thickest ices.

The agreement with previously reported values is good, with small shifts of 2 - 3 cm^{-1}, confirming that at large exposures (*e.g.* $\geq$ 20 L) bulk C_6H_6 is observed. These changes in the peak positions can be easily explained in terms of experimental error (resolution of 2 cm^{-1}), different film thicknesses[10], and techniques[11] (*e.g.* transmission IR instead of RAIRS). Additional features observed at high frequencies above 3000 cm^{-1} could arise from bulk behaviour of crystalline C_6H_6. The difference of 4 cm^{-1} observed for the peak maximum corresponding to the in-plane methyl bending mode ($\delta(CH)_{i.p.}$) is due to its broad band profile when the substrate is solid CH_3OH instead of $CH_3CH_2OCH_2CH_3$. In fact, both the CH bends at 1039 cm^{-1} and 691 cm^{-1} are sharper for C_6H_6/CH_3CH_2O-

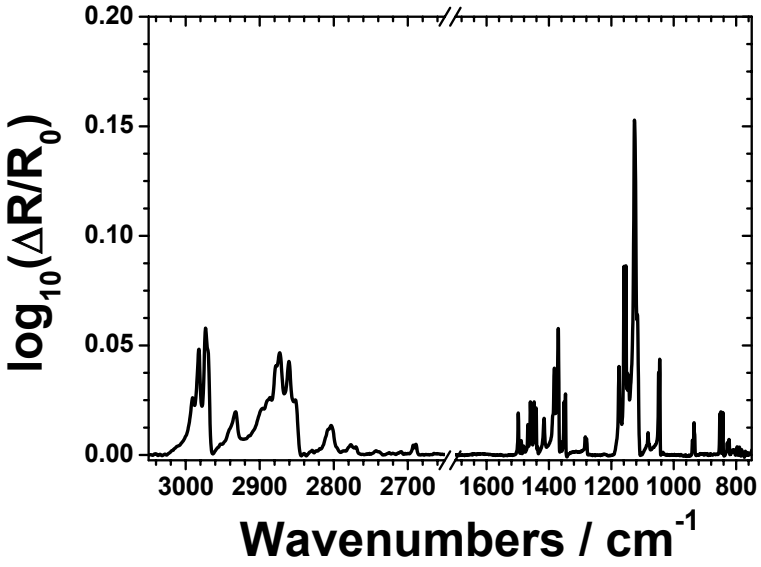

Figure S8: *RAIR spectrum of the multilayer $CH_3CH_2OCH_2CH_3$ film (200 L, $\sim$ 12.1 nm) grown on stainless steel.*

CH_2CH_3 than for C_6H_6/CH_3OH. This might be linked to the growth mechanism of the C_6H_6 film on the two ices. Island formation on CH_3OH is compatible with a larger degree of heterogeneity of polycrystalline C_6H_6, while the aromatic molecules grow as larger and more uniform crystallites on $CH_3CH_2OCH_2CH_3$, therefore displaying sharper peaks.

Assignment	IR Frequencies / cm^{-1}				
	on CH_3OH	on $CH_3CH_2OCH_2CH_3$	on SiO_2 [10]	on Si(111) [11]	on Al [12]
$\delta(CH)_{o.p.}$	689	691	690	688	678
$\delta(CH)_{i.p.}$	1040†	1039	1037	1040	1038
	1029	1033			
$\nu(CC)$	1479	1477	1480	1481	
	1475	1475			
Combination 4	1837	1838	1832	1836	1812
Combination 3	1977	1975	1973	1980	1957
Combination 2	3030	3031	3027	3036	3043
	3037	3037			
Combination 1	3067	3068	3065		3075
$\nu(CH)$	3085	3068	3082	3088	3095
	3092	3092			

Table S2: *List of vibrational modes of C_6H_6 multilayer adsorbed on amorphous CH_3OH or on crystalline $CH_3CH_2OCH_2CH_3$ at base temperature. The superscript † highlights that the frequency assignment can be obtained only by the RAIR spectrum subtracted with the CH_3OH single beam.*

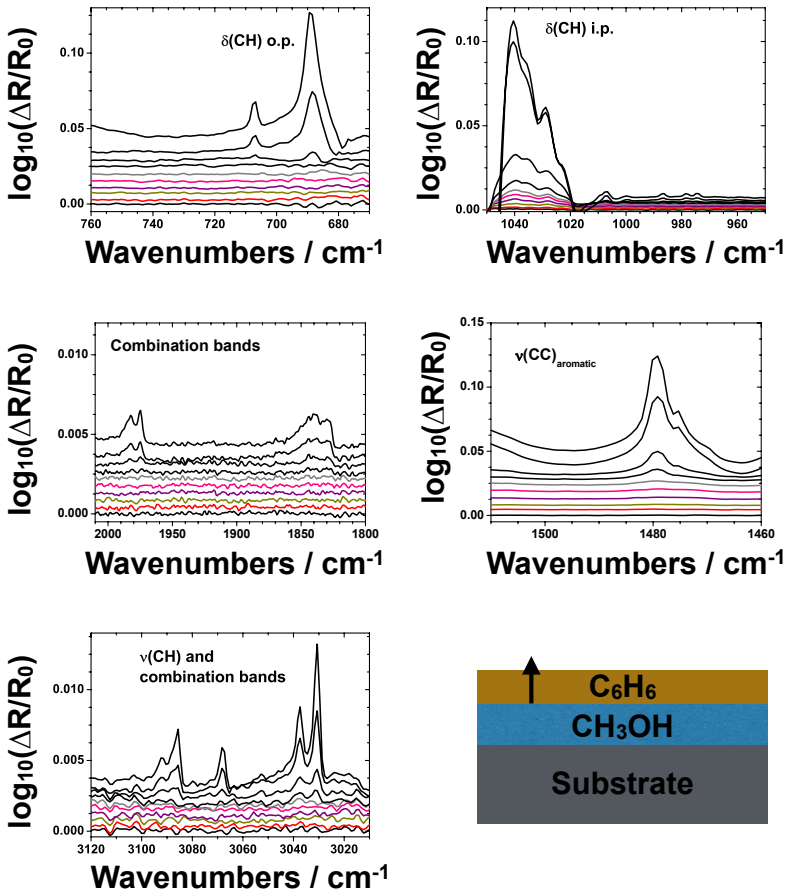

Figure S9: *RAIR spectra of C_6H_6 on a thick CH_3OH film (200 L) highlighting the evolution of the C_6H_6 normal modes at increasing coverages of the aromatic molecule. Spectra have been offset for clarity and subtracted from the pure CH_3OH background. C_6H_6 coverages are: 0. 1 L (in black), 0.2 L (in red), 0.5 L (in dark yellow), 1 L (in violet), 2 L (in pink), and 5L (in dark grey); the spectra relative to higher doses, 10 L, 20 L, 50 L, and 100 L, are reported in black lines. The negative feature, in the region of the $\delta(CH)$* i.p. *is attributed to a decreased IR intensity due to the CH_3OH film as more C_6H_6 is dosed. Note that the initials i.p and o.p. indicate in-plane and out-of-plane vibrational modes respectively. The cartoon at the bottom right corner of the figure is displayed to allow immediate understanding of the experiments performed. The arrow represents the increasing exposure of the aromatic species.*

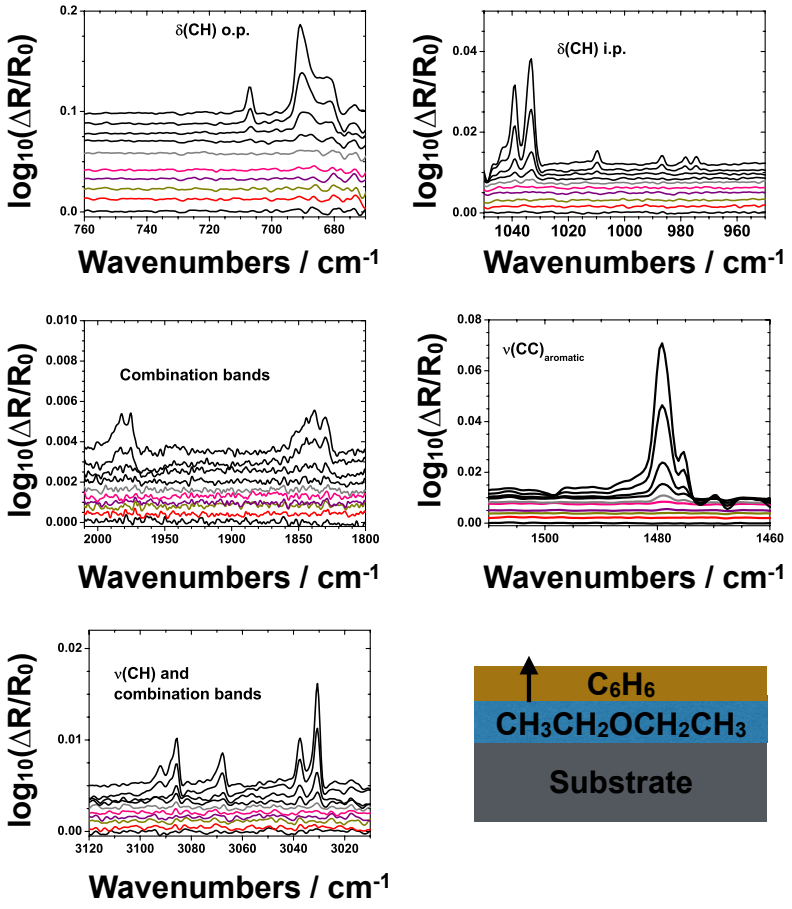

Figure S10: *RAIR spectra of C_6H_6 on a thick $CH_3CH_2OCH_2CH_3$ film (200 L) highlighting the evolution of the C_6H_6 normal modes at increasing coverages of the aromatic molecule. Spectra have been offset for clarity and subtracted from the pure $CH_3CH_2OCH_2CH_3$ background. C_6H_6 coverages are: 0. 1 L (in black), 0.2 L (in red), 0.5 L (in dark yellow), 1 L (in violet), 2 L (in pink), and 5L (in dark grey); the spectra relative to higher doses, 10 L, 20 L, 50 L, and 100 L, are reported in black lines. The negative feature, in the region CH_3 and CH_2 of the bending modes ($\delta(CH)$) is attributed to a decreased intensity of the $CH_3CH_2OCH_2CH_3$ frequencies as more C_6H_6 is dosed. Note that the initials i.p and o.p. indicate in-plane and out-of-plane vibrational modes respectively. The cartoon at the bottom right corner of the figure is displayed to allow immediate understanding of the experiments performed. The arrow represents the increasing exposure of the aromatic species.*

3 Calculations

Computational details and references are reported in the main article. The global minimum for the dimethyl ether (CH_3OCH_3) dimer is shown in **Figure S11a** and its geometry is consistent what was first reported by Tatamitani *et al.*[13]. For this structure, we obtained a binding energy of 13.7 kJ mol^{-1} which is intermediate between the values reported by more recent studies (16.3 kJ mol^{-1}, 12.1 kJ mol^{-1})[14,15] on the same system. Starting form $(CH_3OCH_3)_2$ we have built the corresponding $(CH_3CH_2OCH_2CH_3)_2$ structure and optimised it at the same level of theory. The final geometry is displayed in **Figure S11b**. The binding energy, corrected for the basis set superposition error, is 13.9 kJ mol^{-1} for this dimer, which is almost identical to what found for CH_3OCH_3. This similarity

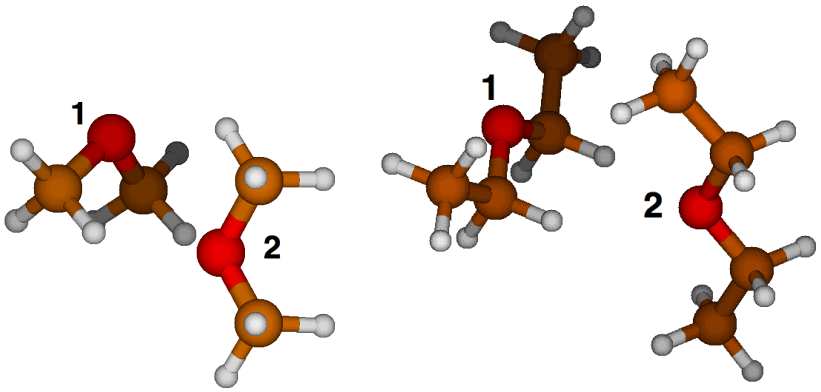

(a) $(CH_3OCH_3)_2$ **(b)** $(CH_3CH_2OCH_2CH_3)_2$

Figure S11: *Global minima (GM) for $(CH_3OCH_3)_2$ and $(CH_3CH_2OCH_2CH_3)_2$. Geometry optimisations were performed at MP2/aug-cc-pVDZ level followed by a single point with aug-cc-pVTZ basis set. Counterpoise (CP) correction was included at each step. The two fragments are labelled as 1 and 2 in both the pairs.*

can be explained by looking at the equilibrium distances of the key interactions. There are four weak CH$\cdots$O interactions in the $CH_3CH_2OCH_2CH_3$ dimer against three of the $(CH_3OCH_3)_2$ dimer. As displayed in **Table S3**, two of the $CH_1\cdots O_2$ interactions have the same equilibrium distances in both the pairs. However, the fragment labelled *2* in the $(CH_3CH_2OCH_2CH_3)_2$ structure has two H-atoms facing the O-atom of the fragment *1* at long distances (3.19 Å) as opposed to $(CH_3OCH_3)_2$ where the $CH_2\cdots O_1$ interaction is established at a shorter equilibrium distance (2.66 Å). The compensation between the number of intermolecular interactions and their equilibrium distances results in similar binding energies for both the two dimers (**Figure S11**).

Interaction	d / Å	
	$(CH_3OCH_3)_2$	$(CH_3CH_2OCH_2CH_3)_2$
$CH_1\cdots O_2$	2.67	2.66
$CH_2\cdots O_1$	2.52	3.19

Table S3: *List of values of the calculated equilibrium distances for the hydrogen bonding interactions established in $(CH_3OCH_3)_2$ and in $(CH_3CH_2OCH_2CH_3)_2$. The subscripts refers to the two fragments as labelled in Figure S11.*

3.1 Cartesian Coordinates

List of XYX coordinates for the optimised geometries (MP2/aug-cc-pVDZ).

Atom	X	Y	Z
C	1.35183300	-0.00116700	1.16353100
O	1.45957000	-0.00031200	-0.25928300
C	2.82479500	0.00090400	-0.66027700
H	0.28183600	-0.00196400	1.40656100
H	1.83270500	-0.89921200	1.59307600
H	1.83155000	0.89702100	1.59406700
H	2.84239100	0.00149000	-1.75732100
H	3.34833600	0.89935700	-0.28506500
H	3.34966100	-0.89716800	-0.28600600
O	-2.06311600	-0.00030000	0.47232300
C	-1.88679500	1.17092600	-0.32184600
C	-1.88690000	-1.17025800	-0.32374200
H	-0.87245700	-1.20155800	-0.75896800
H	-2.03297500	-2.03440700	0.33689400
H	-2.63262400	-1.20669400	-1.13933500
H	-0.87236100	1.20282300	-0.75705300
H	-2.63253500	1.20876500	-1.13736000
H	-2.03275800	2.03401900	0.34019400

Table S4: $(CH_3OCH_3)_2$.

Atom	X	Y	Z
C	1.96494300	-0.00756600	1.58810700
O	1.71740500	-0.00168400	0.18001500
C	2.93478300	0.00292800	-0.56666100
H	2.56089600	-0.90223300	1.85395900
H	2.55886000	0.88609400	1.86179200
H	3.53122400	0.89653500	-0.29847100
H	3.53318700	-0.89168400	-0.30631400
C	0.62733900	-0.01223800	2.30657500
H	0.04353600	-0.90175300	2.03131200
H	0.78524700	-0.01692200	3.39576300
H	0.04151000	0.87836300	2.03924800
C	2.58334100	0.00902200	-2.04418700
H	3.50049900	0.01267100	-2.65220900
H	1.99531300	-0.88351500	-2.30145600
H	1.99339100	0.90250800	-2.29364000
O	-2.17125300	0.00104100	-0.08529300
C	-1.64064500	1.18216000	-0.69143400
C	-1.64186500	-1.17497500	-0.70232800
H	-0.53854900	-1.16487500	-0.62796200
H	-1.91256300	-1.18087000	-1.77697800
H	-0.53733500	1.17016400	-0.61729000
H	-1.91145700	1.19834300	-1.76595000
C	-2.22913500	-2.38414600	0.00472600
H	-1.84706700	-3.31131700	-0.44901900
H	-1.95490900	-2.37603900	1.06956400
H	-3.32573300	-2.38017800	-0.07295700
C	-2.22651000	2.38535000	0.02690100
H	-1.84348400	3.31627900	-0.41826100
H	-3.32312100	2.38330300	-0.05066600
H	-1.95215900	2.36706200	1.09158000

Table S5: $(CH_3CH_2OCH_2CH_3)_2$.

Atom	X	Y	Z
C	-1.21922900	0.70340900	-0.62925500
C	0.00000000	1.40678400	-0.63036500
C	1.21923000	0.70341000	-0.62925400
C	1.21923100	-0.70341000	-0.62925400
C	0.00000000	-1.40678300	-0.63036500
C	-1.21923200	-0.70341000	-0.62925400
H	-0.00000100	2.50013700	-0.63630300
H	2.16586100	1.24982800	-0.62821800
H	2.16586200	-1.24982700	-0.62821800
H	0.00000000	-2.50013700	-0.63630300
H	-2.16586200	-1.24982700	-0.62821900
H	-2.16586000	1.24982700	-0.62822000
O	0.00000100	0.00000000	2.76186500
H	-0.00000100	-0.75309800	2.15525700
H	0.00000200	0.75309800	2.15525700

Table S6: $w1b'_a$.

Atom	X	Y	Z
C	0.78254000	-0.60795500	-1.22151700
C	0.49749100	0.76984500	-1.21597100
C	0.35527800	1.45383700	0.00634800
C	0.49720900	0.75920900	1.22268700
C	0.78225800	-0.61858600	1.21628600
C	0.92550100	-1.30167500	-0.00560100
H	0.13388900	2.52432200	0.01099200
H	0.38239300	1.28965000	2.17134900
H	0.89114600	-1.15800900	2.16067200
H	1.14941500	-2.37173700	-0.01024200
H	0.89165200	-1.13912200	-2.17054500
H	0.38288800	1.30853700	-2.15999700
O	-2.79691600	-0.26872300	-0.00134000
H	-1.93529000	0.17345400	0.00091500
H	-2.56242600	-1.20535600	-0.00582700

Table S7: $w1b'_b$.

Atom	X	Y	Z
C	-2.13201300	-0.70390900	0.00045600
C	-2.13264900	0.70281800	0.00045700
C	-0.91402400	1.40613100	-0.00013400
C	0.30513300	0.70403100	-0.00072600
C	0.30577600	-0.70292600	-0.00072600
C	-0.91275000	-1.40611800	-0.00013500
H	-0.91543900	2.49960700	-0.00013200
H	1.25734900	1.23992100	-0.00113500
H	1.25848300	-1.23793900	-0.00113600
H	-0.91317400	-2.49959500	-0.00013300
H	-3.07876300	-1.25084600	0.00091900
H	-3.07989300	1.24890000	0.00092000
O	3.71645700	-0.00024900	0.00053400
H	4.31134600	0.00088500	0.76144500
H	4.31160000	0.00088700	-0.76017900

Table S8: *w1b″*.

Atom	X	Y	Z
C	0.82802800	1.29041800	-0.70287300
C	0.82817300	1.28953900	0.70442100
C	1.03770900	0.08909600	1.40754100
C	1.25031400	-1.11123700	0.70320800
C	1.25016300	-1.11035700	-0.70474900
C	1.03741400	0.09085500	-1.40753700
H	1.41035600	-2.04451600	1.24908500
H	1.41008600	-2.04295500	-1.25182400
H	1.03254800	0.09015600	-2.50051500
H	0.66328400	2.22305500	-1.24880400
H	0.66354300	2.22149300	1.25155100
H	1.03306800	0.08703000	2.50051800
O	-2.20145500	-0.93986100	-0.00000600
H	-1.23453900	-0.89251800	-0.00000600
C	-2.70015600	0.40069900	-0.00000300
H	-2.38064500	0.95755000	0.89706200
H	-2.38064900	0.95755200	-0.89706800
H	-3.79528500	0.32795800	0.00000000

Table S9: *m1b′*.

Atom	X	Y	Z
C	2.48577300	0.70323600	0.34126800
C	2.48562400	-0.70346900	0.34130000
C	1.34953100	-1.40631200	-0.10070200
C	0.21324800	-0.70357300	-0.54147800
C	0.21339900	0.70377500	-0.54151100
C	1.34982700	1.40629600	-0.10076600
H	1.35068000	-2.49977600	-0.10166500
H	-0.67618300	-1.23929900	-0.88282100
H	-0.67591300	1.23968000	-0.88288500
H	1.35120800	2.49976100	-0.10178600
H	3.36852500	1.24963600	0.68421300
H	3.36826200	-1.25003800	0.68426900
O	-3.07097500	-0.00019200	-0.52762800
H	-3.97738100	-0.00034400	-0.86063900
C	-3.12822800	0.00020900	0.90772000
H	-2.08839200	0.00032800	1.25659400
H	-3.63404800	0.89930700	1.29512500
H	-3.63400900	-0.89869400	1.29563000

Table S10: *m1b″*.

Atom	X	Y	Z
C	-1.55404300	-0.70339500	1.21839100
C	-1.55404400	0.70340900	1.21838300
C	-1.55391100	1.40680100	-0.00000800
C	-1.55404400	0.70339400	-1.21839200
C	-1.55404400	-0.70341000	-1.21838400
C	-1.55391000	-1.40680100	0.00000800
H	-1.55565600	2.50012800	-0.00001600
H	-1.55624800	1.25000100	-2.16525400
H	-1.55624700	-1.25002500	-2.16524100
H	-1.55565400	-2.50012800	0.00001600
H	-1.55624600	-1.25000100	2.16525300
H	-1.55624700	1.25002600	2.16523900
O	3.09217200	-0.00000100	0.00000100
C	2.27945700	1.16855800	-0.00000800
C	2.27945600	-1.16855900	0.00000700
H	2.95560400	2.03296200	-0.00001200
H	1.63259600	1.20399400	-0.89588900
H	1.63259300	1.20400500	0.89587200
H	2.95560200	-2.03296300	0.00001400
H	1.63259200	-1.20399300	0.89588700
H	1.63259500	-1.20400500	-0.89587400

Table S11: *dm1b′*.

Atom	X	Y	Z
C	1.88864000	1.40636400	-0.12009400
C	3.06701900	0.70337200	0.19183400
C	3.06702400	-0.70334500	0.19185700
C	1.88865300	-1.40636100	-0.12004500
C	0.71008300	-0.70368600	-0.43067900
C	0.71007700	0.70366500	-0.43070300
H	1.88982100	-2.49983100	-0.12103000
H	-0.21219600	-1.23901100	-0.67060600
H	-0.21220500	1.23897300	-0.67065100
H	1.88979500	2.49983400	-0.12111700
H	3.98257600	1.24983700	0.43379600
H	3.98258600	-1.24979300	0.43383800
C	-2.52038800	0.00006600	1.25784400
O	-2.56084100	-0.00016700	-0.16639100
C	-3.90628500	0.00003900	-0.63132900
H	-1.46314700	-0.00010400	1.55157400
H	-3.01685700	0.89894800	1.66721900
H	-3.01723400	-0.89846800	1.66752400
H	-4.44708600	0.89860900	-0.28202300
H	-3.87079900	-0.00015900	-1.72779500
H	-4.44746900	-0.89817900	-0.28171200

Table S12: *dm1b″*.

Atom	X	Y	Z
C	0.00000000	1.40683900	-2.15538300
C	1.21839600	0.70340500	-2.15569900
C	1.21839600	-0.70340500	-2.15569900
C	0.00000000	-1.40683900	-2.15538300
C	-1.21839600	-0.70340500	-2.15569900
C	-1.21839600	0.70340500	-2.15569900
H	0.00000000	-2.50021400	-2.15662600
H	2.16527300	-1.25001600	-2.15734000
H	-2.16527300	-1.25001600	-2.15734000
H	2.16527300	1.25001600	-2.15734000
H	-2.16527300	1.25001600	-2.15734000
H	0.00000000	2.50021400	-2.15662600
C	0.00000000	-1.17726100	1.63771700
O	0.00000000	0.00000000	2.44683000
C	0.00000000	1.17726100	1.63771700
C	0.00000000	-2.38615900	2.55645500
H	-0.89150700	-1.17678200	0.98090100
H	0.89150700	-1.17678200	0.98090100
C	0.00000000	2.38615900	2.55645500
H	0.89150700	1.17678200	0.98090100
H	-0.89150700	1.17678200	0.98090100
H	0.00000000	3.31273200	1.96226800
H	-0.89278000	2.37988700	3.19778400
H	0.89278000	2.37988700	3.19778400
H	0.00000000	-3.31273200	1.96226800
H	0.89278000	-2.37988700	3.19778400
H	-0.89278000	-2.37988700	3.19778400

Table S13: *de1b*′.

Atom	X	Y	Z
C	1.14605300	-0.00002000	-0.74852300
C	2.40260400	0.00001100	-1.38157000
C	3.58086900	0.00001300	-0.61236000
C	3.50383800	-0.00001400	0.79232300
C	2.24821300	-0.00004300	1.42727300
C	1.07104900	-0.00004400	0.65673700
H	2.18848700	-0.00006200	2.51913000
H	0.09124500	-0.00006500	1.14159800
H	0.22292300	-0.00002000	-1.33343800
H	2.46392700	0.00002900	-2.47329000
H	4.55652700	0.00003600	-1.10579800
H	4.41934400	-0.00001200	1.38999300
C	-2.62341100	-1.18129600	0.40400600
O	-2.18299600	0.00001600	-0.26781000
C	-2.62336300	1.18133300	0.40402700
C	-2.08609200	2.38495000	-0.35006100
H	-3.72994200	1.19607500	0.44224700
H	-2.25203000	1.17330900	1.44816700
C	-2.08617900	-2.38492200	-0.35009500
H	-3.72999200	-1.19599700	0.44221600
H	-2.25208700	-1.17330000	1.44814900
H	-2.41487700	-3.31444200	0.13874400
H	-2.45625400	-2.38285500	-1.38521800
H	-0.98697600	-2.36631800	-0.36709900
H	-2.41473600	3.31447600	0.13880300
H	-0.98689000	2.36629200	-0.36708700
H	-2.45618800	2.38292100	-1.38517600

Table S14: *de1b″*.

Atom	X	Y	Z
C	-3.11398100	0.16215400	0.45053700
C	-2.72376900	-1.10905100	-0.01360100
C	-1.74260300	-1.22106800	-1.01643700
C	-1.14990600	-0.06393700	-1.55324500
C	-1.54015300	1.20659000	-1.09217700
C	-2.52323400	1.32017100	-0.09138900
H	-3.18195100	-2.00810700	0.40719700
H	-1.42785000	-2.20668400	-1.36812700
H	-0.37217300	-0.15310900	-2.31533300
H	-1.06432300	2.10187900	-1.49913500
H	-2.82501800	2.30692000	0.26993400
H	-3.87650700	0.24997600	1.22919600
O	0.32353800	-0.03363700	1.61761000
H	0.66725000	0.72827500	1.11667700
H	1.21454100	-1.22638600	0.41666100
O	1.78108800	-1.46878700	-0.34586900
H	2.06533500	0.46693100	-0.61215600
O	1.84320900	1.40397300	-0.44849300
H	2.43987600	-2.07240800	0.01948300
H	2.69632000	1.84274800	-0.34050400
H	-0.62923100	-0.01514400	1.44063800

Table S15: *w3b′*.

Atom	X	Y	Z
C	2.28301600	1.05288500	0.58705800
C	3.14544300	-0.06068300	0.53842500
C	3.00584200	-1.01199700	-0.48982600
C	2.00442900	-0.84957600	-1.46658000
C	1.14017300	0.25997200	-1.41562000
C	1.27969000	1.21323100	-0.38893100
H	0.34966900	0.39171200	-2.15767000
H	0.59761600	2.06613500	-0.35769100
H	2.39513300	1.79446000	1.38286500
H	3.92325900	-0.18425900	1.29670800
H	3.67808900	-1.87336000	-0.53148200
H	1.89911900	-1.58740600	-2.26677200
O	-0.04607400	-1.31991600	1.54980400
H	0.66338300	-0.71042700	1.28637100
O	-1.76627200	1.85015500	-1.41404000
O	-2.45642700	-0.11834300	0.58156500
H	-2.57254500	2.09245100	-1.88490300
H	-1.65348000	-0.55815100	0.92618400
H	0.19028200	-2.14452100	1.10451800
H	-2.95007700	0.13200600	1.37197800
H	-2.06347100	1.20234000	-0.74593300

Table S16: *w3b″*.

Atom	X	Y	Z
C	2.34127500	1.24177300	0.10903800
C	2.90743100	0.01260300	0.50192700
C	2.54841600	-1.17342000	-0.16879500
C	1.62464300	-1.13061100	-1.22951700
C	1.06276000	0.09850600	-1.62411100
C	1.41936800	1.28523800	-0.95622700
H	0.33181000	0.12228100	-2.43567700
H	0.96448200	2.23641500	-1.24234300
H	2.61179300	2.16228300	0.63295100
H	3.62491400	-0.01977300	1.32646700
H	2.98596900	-2.12754500	0.13728200
H	1.32423800	-2.05067700	-1.73599100
O	-0.47280900	-0.14282800	1.35305200
C	-0.24399700	-0.97671900	2.50436800
H	0.39532300	0.11032800	0.99410600
H	0.27909400	-1.90321700	2.22048700
H	0.33828900	-0.44331200	3.27119800
H	-1.23078300	-1.22727900	2.91217800
O	-1.53642600	2.48179600	0.56337900
C	-2.39096600	2.11120700	-0.52192500
O	-1.61849700	-1.67051500	-0.89091000
C	-2.97225600	-1.93166600	-0.51378300
H	-1.29571300	1.66335600	1.02715800
H	-1.21418400	-1.15082900	-0.17368100
H	-3.42565800	-2.51538700	-1.32526500
H	-3.03525800	-2.52137700	0.41718700
H	-3.55108700	-1.00106000	-0.38520700
H	-2.56898700	3.01857700	-1.11383200
H	-1.92810800	1.34722600	-1.17024800
H	-3.36431200	1.73089300	-0.16678800

Table S17: *m3b′*.

Atom	X	Y	Z
C	-3.57115200	0.28565000	0.14072200
C	-3.23551200	-1.03725900	-0.20195900
C	-2.02292900	-1.30557500	-0.86430300
C	-1.14583200	-0.25273400	-1.18432600
C	-1.48075700	1.07074000	-0.84117700
C	-2.69344700	1.33845100	-0.17894400
H	-3.91684800	-1.85575700	0.04593500
H	-1.75958300	-2.33308500	-1.12960900
H	-0.20138500	-0.46706700	-1.69074700
H	-0.78822100	1.88115900	-1.08125300
H	-2.95482100	2.36630400	0.08759700
H	-4.51321900	0.49517200	0.65470200
C	-0.26465100	-0.24770800	2.39030100
O	0.98440900	-0.15457200	1.68537900
H	0.97288700	0.63989100	1.11900400
H	-0.20740400	-1.14994200	3.01235900
H	-0.41508900	0.62483000	3.04578400
H	-1.11560800	-0.33735200	1.69766300
H	1.62454400	-1.19985900	0.25372800
O	2.07117700	-1.31901300	-0.61012200
C	3.28714000	-2.04461300	-0.38373900
H	3.80705100	-2.11097100	-1.34773300
H	3.08298100	-3.06456700	-0.02109400
H	3.93959600	-1.52995700	0.34070700
H	2.02025800	0.60009800	-0.78386400
O	1.80369300	1.51527800	-0.51494000
C	3.04093200	2.18719200	-0.24165100
H	3.67421800	2.24865700	-1.14128000
H	3.60448400	1.68881300	0.56482000
H	2.78918700	3.20521400	0.08119700

Table S18: *m3b″*.

Atom	X	Y	Z
C	3.67468600	-0.10677200	-1.23066500
C	3.16557700	1.18957200	-1.03021000
C	2.69781700	1.57254400	0.24011100
C	2.73980500	0.65967500	1.31011000
C	3.25033700	-0.63565100	1.10995400
C	3.71733500	-1.01916600	-0.16054200
H	2.37689700	0.95773200	2.29743200
H	2.30290600	2.58006200	0.39614000
H	3.28474200	-1.34418700	1.94188700
H	3.13343500	1.89896100	-1.86136600
H	4.11502000	-2.02562400	-0.31599500
H	4.03864600	-0.40439900	-2.21764000
C	-1.11359400	0.00136100	0.90494700
O	-1.25597400	-0.76436400	-0.29012700
C	-0.00174200	-1.31963500	-0.67947300
H	-2.10546700	0.40010800	1.15411800
H	-0.74536700	-0.63081000	1.73470600
H	-0.40046600	0.83273900	0.75593700
H	-0.17113000	-1.88312300	-1.60621000
H	0.74790700	-0.52816700	-0.85848200
H	0.38765900	-2.00138900	0.09907000
O	-4.51315500	0.63747800	0.36335400
C	-4.15730600	1.15560300	-0.91669000
C	-4.73847200	-0.76861900	0.28338400
H	-3.83004200	-1.29436300	-0.05953800
H	-5.00552300	-1.10959300	1.29186600
H	-5.57134100	-0.99414600	-0.40824400
H	-3.23477200	0.67889700	-1.29228000
H	-4.97221000	0.99356800	-1.64649200
H	-3.99359800	2.23389500	-0.79338000

Table S19: *dm2b′*.

Atom	X	Y	Z
C	-1.51352200	-1.49024000	-0.06530700
C	-1.93778400	-0.97753800	1.17408200
C	-2.77366700	0.15369700	1.22267100
C	-3.18660000	0.77430100	0.02955000
C	-2.76591500	0.26071600	-1.21132100
C	-1.93071900	-0.87051000	-1.25754700
H	-3.08868400	0.74089100	-2.13914900
H	-1.59985900	-1.26725600	-2.22117700
H	-0.84606100	-2.35447300	-0.10676700
H	-1.61911100	-1.45852100	2.10307400
H	-3.10251500	0.54994500	2.18722000
H	-3.83599000	1.65314700	0.06628600
O	1.90565500	-1.87151200	-0.15260700
C	3.08292300	-1.48675700	-0.86084400
C	2.02038300	-1.51670600	1.22448600
H	1.08765700	-1.82270100	1.71597100
H	2.87032000	-2.04436100	1.69581700
H	2.15911200	-0.42743800	1.34065600
H	3.97086800	-2.01211800	-0.46319400
H	2.93517700	-1.77137900	-1.91051800
H	3.24721300	-0.39680500	-0.78956200
O	1.89996000	1.82202000	0.00502200
C	0.66482700	1.38729500	-0.56694200
C	1.82325000	3.19215100	0.37898800
H	-0.16825400	1.49997000	0.15113100
H	0.42939800	1.96645900	-1.47927000
H	0.77799600	0.32598500	-0.81864100
H	2.79261600	3.46779300	0.81337800
H	1.62026400	3.83306000	-0.49886500
H	1.02588000	3.35527700	1.12739800

Table S20: *dm2b″*.

4 Acknowledgments

The authors would like to acknowledge the use of the EPSRC UK National Service for Computational Chemistry Software (NSCCS) at Imperial College London and contributions from its staff in carrying out this work.

References

[1] D. A. King, *Surf. Sci.*, 1975, **47**, 384–402.

[2] G. Attard and C. Barnes, *Surfaces*, Oxford University Press, 2011.

[3] P. A. Redhead, *Vacuum*, 1962, **12**, 203.

[4] R. S. Smith, J. Matthiesen and B. D. Kay, *J. Phys. Chem. A*, 2014, **118**, 8242.

[5] C. J. Craven, P. D. Hatton, C. J. Howard and G. S. Pawley, *J. Chem. Phys.*, 1993, **98**, 8236–8243.

[6] A. S. Bolina, A. J. Wolff and W. A. Brown, *J. Chem. Phys.*, 2005, **122**, 044713.

[7] D. Marchione, *PhD thesis*, Heriot-Watt University, 2015.

[8] F. C. Calaza, T. L. Chen, D. R. Mullins and S. H. Overbury, *Top. Catal.*, 2011, **54**, 56.

[9] J. M. Meyers and S. C. Street, *Langmuir*, 1996, **12**, 1511.

[10] J. D. Thrower, *PhD thesis*, Heriot-Watt University, 2009.

[11] G. Strazzulla and G. A. Baratta, *Astron. Astrophys.*, 1991, **241**, 310.

[12] R. Ruiterkamp, Z. Peeters, M. H. Moore, R. L. Hudson and P. Ehrenfreund, *Astron. Astrophys.*, 2005, **440**, 391.

[13] Y. Tatamitani, B. Liu, J. Shimada, T. Ogata, P. Ottaviani, A. Maris, W. Caminati and J. L. Alonso, *J. Am. Chem. Soc.*, 2002, **124**, 2739–2743.

[14] A. Karpfen and E. S. Kryachko, *Phys. Chem. Lett.*, 2006, **431**, 428–433.

[15] B. L. Yoder, K. B. Bravaya, A. Bodi, A. H. C. West, B. Sztáray and R. Signorell, *J. Chem. Phys.*, 2015, **142**, 114303–1.